Low-intensity open-field blast exposure effects on neurovascular unit ultrastructure in mice

Chao Li[1,3†], Shanyan Chen[1,2†], Heather R. Siedhoff[1,2], DeAna Grant[4], Pei Liu[5], Ashley Balderrama[1,2], Marcus Jackson[1], Amitai Zuckerman[1,2], C. Michael Greenlief[5], Firas Kobeissy[6,10], Kevin W. Wang[6,10], Ralph G. DePalma[7,8], Ibolja Cernak[9], Jiankun Cui[1,2] and Zezong Gu[1,2*]

Abstract

Mild traumatic brain injury (mTBI) induced by low-intensity blast (LIB) is a serious health problem affecting military service members and veterans. Our previous reports using a single open-field LIB mouse model showed the absence of gross microscopic damage or necrosis in the brain, while transmission electron microscopy (TEM) identified ultrastructural abnormalities of myelin sheaths, mitochondria, and synapses. The neurovascular unit (NVU), an anatomical and functional system with multiple components, is vital for the regulation of cerebral blood flow and cellular interactions. In this study, we delineated ultrastructural abnormalities affecting the NVU in mice with LIB exposure quantitatively and qualitatively. Luminal constrictive irregularities were identified at 7 days post-injury (DPI) followed by dilation at 30 DPI along with degeneration of pericytes. Quantitative proteomic analysis identified significantly altered vasomotor-related proteins at 24 h post-injury. Endothelial cell, basement membrane and astrocyte end-foot swellings, as well as vacuole formations, occurred in LIB-exposed mice, indicating cellular edema. Structural abnormalities of tight junctions and astrocyte end-foot detachment from basement membranes were also noted. These ultrastructural findings demonstrate that LIB induces multiple-component NVU damage. Prevention of NVU damage may aid in identifying therapeutic targets to mitigate the effects of primary brain blast injury.

Keywords Open-field blast, Mild traumatic brain injury, Neurovascular unit, Transmission electron microscopy, Ultrastructural abnormalities

†Chao Li and Shanyan Chen contributed equally to this work.

*Correspondence:
Zezong Gu
guze@health.missouri.edu
[1]Department of Pathology & Anatomical Sciences, University of Missouri School of Medicine, One Hospital Drive, Medical Science Building, M741, Columbia, MO 65212, USA
[2]Truman VA Hospital Research Service, Columbia, MO 65201, USA
[3]Department of Rehabilitation Medicine, The Third Affiliated Hospital, Sun Yat-sen University, Guangzhou, Guangdong 510630, China
[4]Electron Microscopy Core Facility, University of Missouri, Columbia, MO 65211, USA
[5]Charles W. Gehrke Proteomic Center, University of Missouri, Columbia, MO 65211, USA
[6]Department of Neurobiology, Center for Neurotrauma, Multiomics & Biomarkers (CNMB), Neuroscience Institute, Morehouse School of Medicine, Atlanta, GA 30310-1458, USA
[7]Office of Research and Development, Department of Veterans Affairs, Washington, DC 20420, USA
[8]Department of Surgery, Uniformed Services University of the Health Sciences, Bethesda, MD 20814, USA
[9]Department of Biomedical Sciences, Mercer University School of Medicine, Macon, GA 31207, USA
[10]Atlanta VA Medical and Rehab Center, Decatur, GA 30033, USA

Introduction

Blast-induced traumatic brain injury (bTBI) is of particular concern among military personnel.

Explosions cause complex blast injuries, including primary, secondary, tertiary, and quaternary blast injuries [1]. Primary blast injury of the brain as a unique clinical entity due to the direct energy transfer of the shockwaves [2] was recently released by the Centers for Disease Control and Prevention (CDC) with the FY2023 ICD-10-CM code S06.8 A [3] for the related classifications of the disease. Mild TBI (mTBI) caused by low-intensity blast (LIB) exposure of service members during deployment and in non-combat settings such as military occupational training has been increasingly recognized [2, 4]. The Traumatic Brain Injury Center of Excellence (TBICoE), US Defense Department (DoD), recently reported that 82.3% of 453,919 military TBIs during the interval 2000–2021 Q4 were mTBI [5]. This injury, most often without loss of consciousness, associates with a greater than a two-fold increase in the risk of later dementia [6]. Lifelong disabilities impose immense burden on affected Service members and Veterans, their families, and society. An urgent need to better understand and treat the consequences of these "invisible injuries".

The neurovascular unit (NVU) is an anatomical and functional structure comprised of multiple components, including endothelial cells, tight junctions, pericytes, basement membranes, perivascular astrocytes, microglia, neurons, and extracellular matrix. The NVU is central to the interactions between microvessels and neuronal cells in regulating cerebral blood flow and maintaining the integrity of the blood–brain barrier (BBB) [7, 8]. Disturbances of NVU homeostasis occur in many neurological diseases, including ischemic stroke and TBIs [9–14]. Increased BBB permeability induced by single or repeated blast exposure (shock tubes at 72 to 137 kPa) has been documented by leakage of exogenous chemical tracers, proteomic analyses, and MRI imaging [15–19]. Structural abnormities of the NVU occurred post-blast exposure generated in shock tubes (74.5 kPa), including swollen astrocyte end-feet, disrupted pericytes and endothelial cells, as well as abnormally shaped capillary lumens [20, 21]. Blast-induced NVU impairments have been postulated to include oxidative stress, matrix metalloproteinases (MMP) activation, inflammation, and increased glial cell reactivity [19, 20, 22].

Our previous observation using the open-field LIB mouse model—entailing elimination of head movement—in an open-field environment revealed that single blast exposure with a peak overpressure of 46.6 kPa did not result in gross microscopic damage or necrosis in the brain, while TEM identified multiple ultrastructural abnormalities of axonal myelin sheaths, mitochondria and synapses [23–25]. This study provides quantitative and qualitative TEM analyses of multi-component NVU abnormalities uniquely induced by open-field LIB exposure. We detailed morphologic features and quantitative analyses of the microvessel lumens, pericytes, endothelial cells, basement membranes, astrocyte end-feet, and tight junctions using TEM at 7- and 30-days DPI, as well as proteomic assays at 24 h post-injury. We also quantified neurofilaments light chain (Nf-L) and glial fibrillary acidic protein (GFAP) in mouse brain tissues and plasmas at acute, subacute and chronic stages post-LIB injury, which were also used in testing patients with TBI as the FDA-approved peripheral blood biomarkers [26, 27]. In combining these multidisciplinary assessments, we hypothesized that a single LIB in open field results in ultrastructural NVU impairments.

Materials and methods

Animals and open-field LIB setting

All animal experiments were performed in accordance with the University of Missouri-approved protocols for the Care and Use of Laboratory Animals and the Animal Research: Reporting of In Vivo Experiments (ARRIVE) guidelines. Two-month-old male C57BL/6J mice (The Jackson Laboratory, Bar Harbor, ME) were used. Mice were housed in groups of 5 per cage with a 12-hour light / dark cycle in home-cages containing bedding, with *ad libitum* access to food and water. LIB exposure was conducted at the Missouri University of Science & Technology, as previously reported [23–25, 28–32]. Animals were randomly assigned into the LIB-exposed group and the sham group. The investigators performing experimental analyses were double-blinded about the group assignments of the mice. Mice were anesthetized with an intraperitoneal (i.p.) injection of 5 μL / g body weight of ketamine / xylazine mixture (25 mg / mL ketamine and 1.25 mg / mL xylazine). Mice were placed in metal mesh animal holders in prone orientation at 3-meter distance away from the detonation of a 350 g C4 explosive. The explosion generated a magnitude of 46.6 kPa peak overpressure with a maximal impulse of 60 kPa × ms. No mouse head- or body-movements were observed. Thus, the resulting LIB-induced TBI was, in all likelihood, attributable to the primary blast effects, but not inertial brain injury. The sham group underwent identical handling and anesthesia procedures, only without LIB exposure. After recovery from anesthesia, mice were monitored for at least 15–30 min and allowed access to food and water *ad libitum*.

TEM imaging

Animals used for the TEM study were sacrificed at 7 and 30 DPI. Samples were collected and processed as previously described [24, 25]. Briefly, anesthetized mice were perfused transcardially with saline containing heparin at

room temperature, and then with cold 4% paraformaldehyde. One-mm thick brain sections were cut with the brain matrix (Ted Pella, Inc., Altadena, CA, USA) and fixed with primary fixative solution (100 mM sodium cacodylate, 2% glutaraldehyde, and 2% paraformaldehyde, Electron Microscopy Sciences, Hartfield, PA, USA). Brain sections were further stereologically cut into 1 mm^3 tissue from cerebral cortices under the light microscope. Tissues were stored in 0.1 M NaCacodylate buffer (pH=7.4) containing 0.13 M sucrose and then embedded with 1% osmium tetroxide (Ted Pella, Inc. Redding, California) in Cacodylate buffer. Each tissue block was trimmed approximately 150 μm deep and the surrounding tissues to avoid potential artifacts. Approximately 250 μm × 200 μm tissue blocks were selected for sectioning at 85 nm thickness using an ultramicrotome (Ultracut UCT, Leica Microsystems, Germany) and a diamond knife (Diatome, Hatfield PA). Images were acquired with a JEOL JEM 1400 transmission electron microscope (JEOL, Peabody, MA) at 80 kV on a Gatan Ultrascan 1000 CCD (Gatan, Inc, Pleasanton, CA).

Quantitative analyses of NVU components in TEM images

Electron micrographs of microvessels from mouse brains were collected for analysis using Image J software. Criteria for microvessel selections and quantitative methods were based on previous reports [33–37]. Inclusion criteria for microvessels included: (1) intact vessels; (2) diameters<8 mm; and (3) images not containing nuclei of endothelial cells or pericytes. Numbers of microvessels meeting criteria and included for quantitative analyses: 7-day sham, n=27 from 2 mice; 7-day LIB, n=48 from 4 mice; 30-day sham, n=32 from 3 mice; 30-day LIB, n=33 from 4 mice. Microvessel lumens, endothelial cells, pericytes, and astrocyte end-feet were manually traced using Image J software to calculate areas. Relative areas of endothelial cells, pericytes, and astrocyte end-feet were normalized with lumen areas of individual microvessels, with the formulas as follows:

Relative pericyte areas=pericytes areas / lumen areas;
Relative endothelial cell areas=endothelial cell areas / lumen areas;
Relative astrocyte end-foot areas=astrocyte end-foot areas / lumen areas.

Lumen ratios were defined as the longest diameter in the lumen circle / the perpendicular bisector of the long diameter. Pericyte coverages of endothelial cells were calculated as the percentages of total lengths of inner pericyte processes around each microvessel relative to perimeters of endothelial cells. Astrocyte end-foot coverages of the microvessels were calculated as the percentages of the total length of inner end-foot processes around each microvessel relative to the perimeters of the basement membranes. Vacuolations of the endothelial cells were quantified by the numbers of vacuoles (diameters>50 nm) per 10 μm of the endothelial cell circumferences. Basement membrane thickness was measured in straight lines between the inside and outside edges of the basement membranes at four cardinal points. Cardinal points were chosen typically at the 3, 6, 9, and 12 o'clock positions, avoiding areas where the basement membranes have been expanded by the presence of pericytes. Tight junctions were visualized in high-magnification images: 7-day sham, n=25 from 2 mice; 7-day LIB, n=55 from 4 mice; 30-day sham, n=41 from 3 mice; 30-day LIB, n=33 from 4 mice. Tight junctions with discontinuities, membrane-bound spaces, and vacuole formations were classified as abnormal.

Immunofluorescence

Animals used for the immunofluorescence study were sacrificed at 7 DPI (sham, n=6; LIB, n=6). Mouse brains were dissected and cut into serial coronal sections of 40-μm thickness, then post fixed with 4% paraformaldehyde as previously described [11, 13]. Sections were immunostained with the following antibodies: aquaporin-4 (AQP-4) (A5971, MilliporeSigma, Burlington, MA, USA), glial fibrillary acidic protein (GFAP) (G3893, MilliporeSigma, Burlington, MA, USA), goat anti-rabbit Alexa488 (A-110,034, Thermo Fisher Scientific, Waltham, MA, USA) and goat anti-mouse Alexa594 (A-11,005, Thermo Fisher Scientific, Waltham, MA, USA), as well as nuclear DNA dye Hoechst 33,342. Fluorescence images were taken with a Leica DMI 6000B microscope (Leica Microsystem). 3D deconvolution was used to enhance the sharpness and contrast of fluorescent images with the LAS AF analysis tools.

Protein extraction, digestion, and mass spectrometry (MS) analysis

Animals used for the proteomic study were sacrificed at 24 h post-injury (sham, n=5; LIB, n=5). Mouse brains were dissected and processed as described previously [29]. The temporal halves of the cortex tissues were collected for analysis. Lyse sample buffer (2% sodium dodecyl sulfate [SDS], 0.5 M tetraethylammonium bicarbonate [TEAB], pH 8.5, protease inhibitor cocktails) was added to each tissue sample. Samples were homogenized using Glas-Col stringer 099 C K43 (Glas-Col LLC, IN) and then centrifuged at 17,000 × g for 20 min at 4 °C. Supernatants were collected and then precipitated by cold acetone. Protein pellets were suspended in 6 M urea, 2 M thiourea, and 100 mM ammonium bicarbonate. Protein concentrations were determined using Pierce 660 nm Protein Assay (Thermo Fisher Scientific) according to

the manufacturer's protocol. An equal amount of protein (30 µg) from each sample was reduced, alkylated, digested by sequential LysC, and trypsin, and purified by C18 Tips as described previously [38]. Purified peptides were then lyophilized and resuspended in 5% acetonitrile, 0.1% formic acid. Resuspended peptides were analyzed using Bruker timsTOF pro mass spectrometer as previously described with 90 min LC gradient: initial condition 2% B (A: 0.1% formic acid in water, B: 99.9% acetonitrile, 0.1% formic acid), followed by 26 min ramp to 17% B, 17–25% B over 36 min, 25–37% B over 15 min, a gradient of 37% B to 80% B over 6 min, hold at 80% B for 7 min [38]. The timsTOF pro was operated in parallel accumulation–serial fragmentation (PASEF) mode. The duty cycle was locked to 100%. Ion mobility coefficient ($1 / K_0$) value was set from 0.6 to 1.6 Vs cm^{-2}. MS data were collected over m / z range of 100 to 1700. During MS / MS data collection, each TIMS cycle contained one MS and ten PASEF MS / MS scans. The exclusion was active after 0.4 min.

Quantification of Nf-L and GFAP levels in brain tissue and plasma

Other cohorts of mice were sacrificed at 24 h, 7 days, and 3 months post-LIB injury. After the collection of circulating blood to prepare plasma, mouse brains were dissected and processed as described previously [29]. The temporal halves of the cortex tissues were collected for biomarker analysis. Brain tissue lysate was prepared by first homogenizing the cortex tissue (about 150–200 mg) with cold lysis buffer (20 mM Tris-HCl, 150 mM NaCl, 1% Triton-X100 (v/v), 5 mM EDTA and 1x protease/phosphatase inhibitor cocktail (Sigma) for 30 s x 2, then centrifuged at 4˚C at 1,500 rpm for 5 min. The supernatant was collected and assayed for protein concentration. Most of the tissue or plasma sample numbers were 4–6 per group and some up to 10 with the detailed sample numbers of each group listed in figure legends. Thereafter the protein concentration was adjusted to 1 µg/µL. For biomarker assay, 25 µL of either tissue lysate or plasm samples were diluted ¼ with sample diluent (Quanterix). We assayed GFAP and Nf-L (Quanterix Simoa) with an ultrasensitive immunoassay using digital array technology (S̲ingle M̲olecule A̲rrays, SiMoA)-based Human Neurology 4-Plex B assay (N4PB; Item 103,345). SiMoA assays were run on the SR-X benchtop assay platform (Quanterix Corp., Lexington, MA) at the Morehouse School of Medicine laboratory (Atlanta, GA) accordingly to the manufacturer's instructions [26, 27]. The lower limit of quantitation (LLOQ), limit of detection (LOD), and dynamic range are 9.38 pg/mL, 1.32 pg/mL, and 1.32 to 250,000 pg/mL for GFAP. Interassay and intraassay % Coefficients of Variability (CV) are 7.5–10.8% for GFAP. The LLOQ, LOD, and dynamic range are 0.625 pg/mL,

0.097 pg/mL, and 0.0971-10,000 pg/mL for Nf-L, respectively. Interassay and intraassay % CV are 4.6–6.9% and 3.5–7.5%, respectively for Nf-L.

Statistical analyses

Data were analyzed using Prism software 9 (GraphPad Software, La Jolla, CA). Sample size determination was based on previous publications [24, 25]. For statistical analyses of TEM studies, the D'Agostino-Pearson test was used for normality as recommended by Prism. Data adhering to normal distribution were analyzed with unpaired two-tailed *t*-test and depicted as mean±SD; data adhering non-normally distributed data were analyzed with two-tailed Mann-Whitney nonparametric tests and presented as the median and interquartile range (being the 25th and 75th percentile). For statistical analyses of proteomic datasets, the Shapiro-Wilk test was used for normality as the appropriate method for small sample sizes. Data adhering to normal distribution were analyzed with unpaired two-tailed *t*-test and depicted as mean±SD. For statistical analyses of Nf-L and GFAP levels, the Shapiro-Wilk test was used for normality as the appropriate method for small sample sizes. Data adhering to normal distribution were analyzed with unpaired two-tailed *t*-test and depicted as mean±SD; data adhering to non-normally distributed data were analyzed with two-tailed Mann-Whitney nonparametric tests and presented as the median and interquartile range (being the 25th and 75th percentile). Differences were considered significant at p<0.05.

Results

Luminal irregularities of microvessels in mouse brains post-LIB exposure

Abnormal constrictions of blood vessels (vasospasms) in brains have been well documented in ischemic stroke, as well as TBIs with incidences ranging from 19 to 68% [39, 40]. The present ultrastructural study showed that microvessels in LIB-exposed mouse brains exhibited varying irregularities of luminal circularity compared to sham controls at 7 DPI (Fig. 1a). Detailed quantitative analyses revealed that microvessel lumen areas were significantly smaller by 42.0% (mean value) and lumen ratios significantly higher by 116.0% (mean value) in LIB-exposed mice compared to sham controls at 7 DPI. Interestingly, at 30 DPI these patterns were not identical, however significantly larger lumen areas and lower lumen ratios in LIB-exposed mice were observed (Fig. 1b).

In a continuum of biomarkers released at different time points following the TBI, BBB damage-related proteins can be identified in the acute phase (within 24 h) post injury [41].

To further investigate molecular biosignatures of instant reactions of LIB exposure leading to the luminal
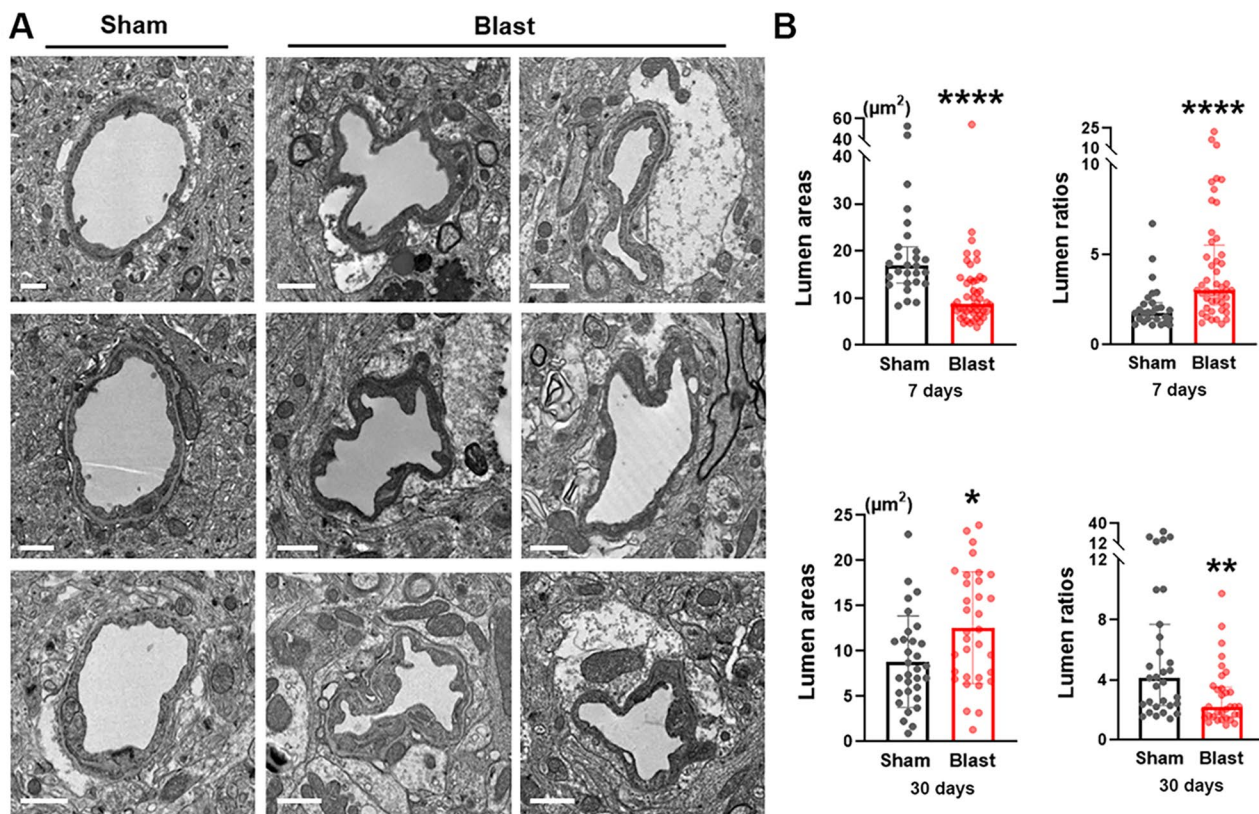
Fig. 1 Ultrastructural abnormalities of luminal circularities in mouse brains post-LIB exposure. (**a**) Representative electron micrographs of microvessels in sham controls and LIB-exposed mice at 7 DPI. Scale bar, 1 µm. (**b**) Quantifications of electron micrographs reveal lumen areas and lumen ratios in sham controls and LIB-exposed mice at 7 and 30 DPI. *, $p < 0.05$, **, $p < 0.01$ and ****, $p < 0.0001$. Lumen areas at 30 DPI are expressed as mean ± SD; other data are expressed as median and interquartile range

irregularities, profiles of global proteomes were analyzed using label-free quantitative mass spectrometry in brain samples collected at 24 h post-LIB exposure. Identified proteins were examined by searching the published proteome of mouse cerebral arteries [42]. Four proteins involved in vasomotor functioning were significantly downregulated in LIB-exposed mice: nitric oxide synthase (NOS) (S4R255), tyrosine 3-monooxygenase (TY3H), serine / threonine-protein phosphatase (fragment) (A0A0G2JFF1) and serine / threonine-protein phosphatase PP1-alpha catalytic subunit (PP1A). In addition, two proteins involved in vasomotor were significantly upregulated in LIB-exposed mice, including calcium-transporting ATPase, two isoforms (F8WHB1 and S4R1C4) (Supplemental Fig. 1).

Degeneration of pericytes in mouse brains post-LIB exposure

Pericytes regulate diameters and blood flow in brain microvessels [43, 44]. Literature reports that pericytes cover approximately 30% of the outer perimeters of endothelial cells in adult mice [45], which is consistent with the 31.5% average pericyte coverage in sham control mice

of our current study (Fig. 2b). Loss of pericytes is involved in the pathophysiological processes of neurodegenerative diseases, such as poststroke dementia, vascular dementia, and Alzheimer's disease [46]. The present ultrastructural study showed pericytes in LIB-exposed mice did not differ significantly from sham controls at 7 DPI (Fig. 2b). By contrast, relative pericyte areas were significantly less by 40.2% (mean value) and pericyte coverages significantly reduced by 23.7% (mean value) in LIB-exposed mice compared to sham controls at 30 DPI (Fig. 2a and b). Vacuole formations were also observed in pericytes in LIB-exposed mice at 7 and 30 DPI (Fig. 2c$_{1-3}$).

Endothelial cell swellings in mouse brains post-LIB exposure

Endothelial cells are a single layer of flat cells covering the inner surface of blood vessels. Swellings of endothelial cells have been identified in cerebral ischemia and associated with the breakdown of the BBB [47]. The present ultrastructural study showed endothelial cell swellings and vacuole formations in LIB-exposed mice at 7 DPI (Fig. 3a and b). Quantitative analyses revealed significantly larger relative endothelial cell areas by 67.2%
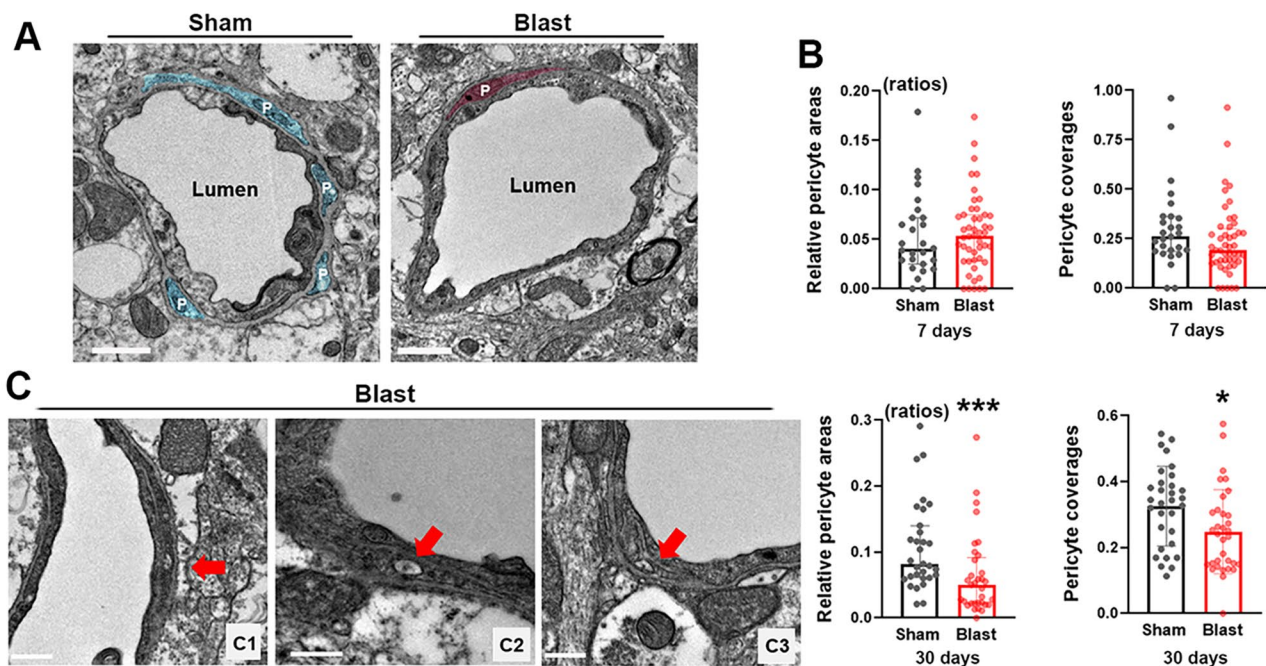
Fig. 2 Ultrastructural abnormalities of pericytes in mouse brains post-LIB exposure. (**a**) Representative electron micrographs of microvessels in sham controls and LIB-exposed mice. Pericytes (P) are highlighted in blue in sham controls and pink in LIB-exposed mice at 30 DPI. Scale bar, 1 μm. (**b**) Quantifications of electron micrographs reveal pericyte coverages and relative pericyte areas in sham controls and LIB-exposed mice at 7 and 30 DPI. *, p < 0.05 and ***, p < 0.001. Pericyte coverages at 30 DPI are expressed as mean ± SD; other data are expressed as median and interquartile range. (**c**) Red arrows indicate vacuoles within pericytes in LIB-exposed mice at 7 (c_1) and 30 (c_2, c_3) DPI. Scale bar, 0.5 μm

(mean value) and significantly higher densities of vacuoles by 55.4% (mean value) in LIB-exposed mice compared to sham controls at 7 DPI (Fig. 3c). By contrast, LIB-exposed mice showed slightly reduced relative endothelial cell areas and no significant differences in vacuole densities at 30 DPI (Fig. 3c). We also identified other ultrastructural abnormalities of endothelial cells in LIB-exposed mice, including inconsistent densities of endothelial cells, abnormal internal bulges, and detachments of endothelial cells at 7 and 30 DPI (Fig. $3d_{1-4}$).

Thickening of basement membranes in mouse brains post-LIB exposure

Structural changes of the basement membranes of NVU, including degradation, diffusion, electron-lightening, and thickening have been identified as important features seen in neurodegenerative diseases, such as ischemic stroke [48]. In this study assessing ultrastructural changes, LIB exposure led to thickening of basement membranes (Fig. 4a). Significantly thicker basement membranes of 0.084 and 0.080 μm (mean value) were found in LIB-exposed mice at 7 and 30 DPI, compared to 0.065 and 0.062 μm (mean value) in sham control mice respectively (Fig. 4b). In addition, compared to basement membranes in sham control mice (Fig. $4c_1$), multiple ultrastructural abnormalities were also observed in LIB-exposed mice, including bulges, fragmentations,

corrugations, and vacuole formations at 7 and 30 DPI (Fig. $4c_{2-6}$).

Astrocyte end-foot swellings and detachments in mouse brains post-LIB exposure

In the present ultrastructural study, swellings of astrocyte end-feet were observed in LIB-exposed mice at 7 DPI (Fig. 5a), in agreement with previous studies on bTBI and ischemic stroke [21, 49]. Quantitative analyses revealed significantly larger relative astrocyte end-foot areas by 75.9% (mean value) at 7 DPI and significantly increased astrocyte end-foot coverages by 27.4% (mean value) at 30 DPI in LIB-exposed mice compared to sham controls (Fig. 5b). Astrocyte end-feet were also laden with vacuoles in LIB-exposed mice at 7 DPI (Fig. 5c).

We further investigated whether astrocyte end-foot detachments [50–52] were involved in LIB-induced mTBI. We observed enlarged spaces between astrocyte end-feet and basement membranes (Fig. $5d_{1-3}$), as well as between adjacent end-feet (Fig. $5d_4$). Quantitative analyses revealed significantly increased distances between astrocyte end-feet and basement membranes by 218.0% and 133.5% (mean values) in LIB-exposed mice compared to sham controls at 7 and 30 DPI respectively (Fig. 5e).

Reactive astrocytes in response to TBIs occur in neuroinflammation and progression of neurodegenerative
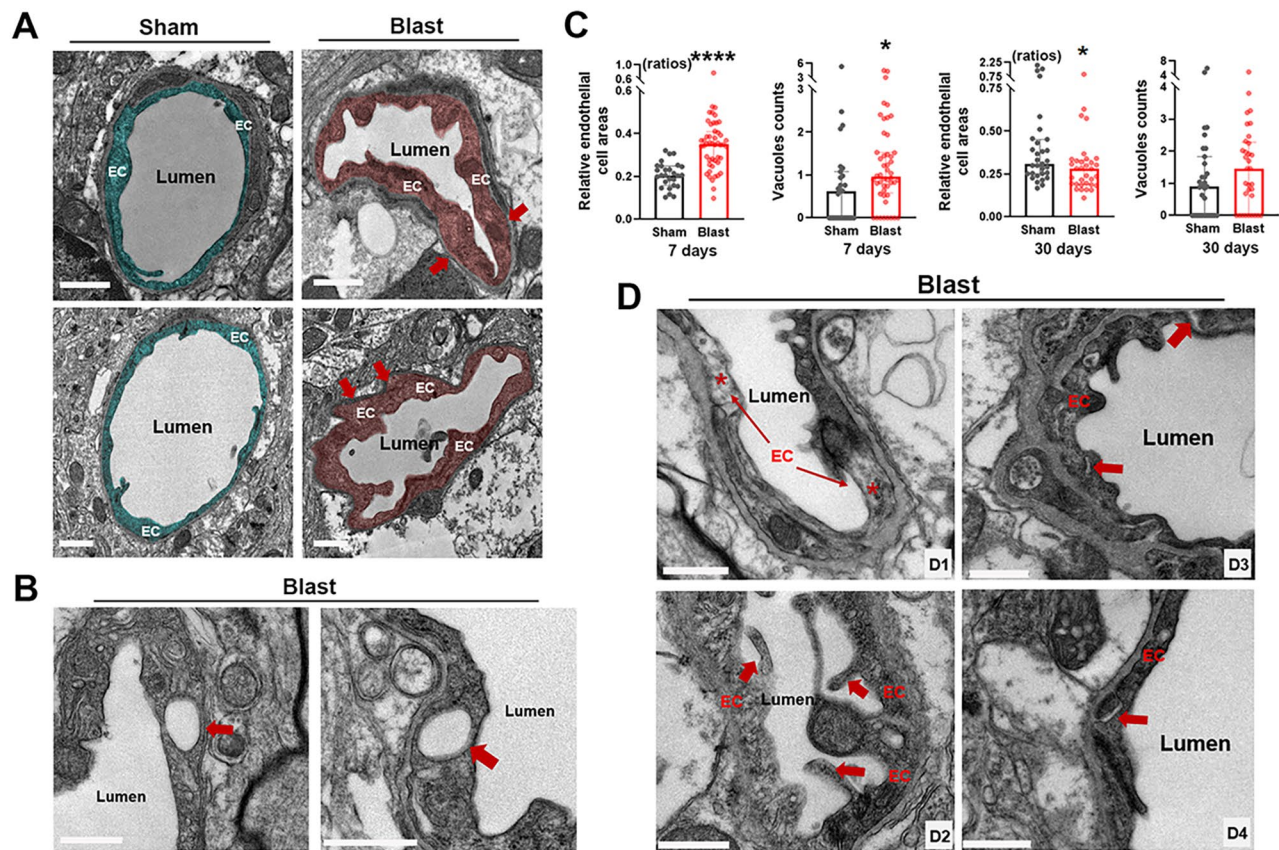
Fig. 3 Ultrastructural abnormalities of endothelial cells in mouse brains post-LIB exposure. (**a**) Representative electron micrographs of microvessels in sham controls and LIB-exposed mice. Endothelial cells (EC) are highlighted in blue in sham controls and pink in LIB-exposed mice at 7 DPI. Scale bar, 1 μm. (**b**) Red arrows indicate vacuoles within endothelial cells in LIB-exposed mice at 7 DPI. Scale bar, 1 μm. (**c**) Quantifications of electron micrographs reveal relative endothelial cell areas and densities of vacuoles in sham controls and LIB-exposed mice at 7 and 30 DPI. *, $p < 0.05$ and ****, $p < 0.0001$. Data are expressed as median and interquartile range. (**d**) Red arrows and red asterisks indicate ultrastructural abnormalities of endothelial cells (EC) in LIB-exposed mice, including density inconsistencies (d_1) and abnormal bulges (d_2) at 7 DPI, as well as endothelial cell detachments (d_3 at 30 DPI and d_4 at 7 DPI). Scale bar, 0.5 μm

diseases, as identified in our previous non-blast TBI study, as well as bTBI studies from other groups [17, 53, 54]. Aquaporin-4 (AQP-4) are water channels located within the astrocyte end-feet surrounding cerebral blood vessels. We studied perivascular astrocytes using the colocalization of AQP-4 and glial fibrillary acidic protein (GFAP) immunoreactivity. In LIB-exposed mice at 7 DPI, perivascular astrocytes showed morphological changes of soma hypertrophy and increased expression of GFAP, while non-reactive astrocytes occurred in sham controls (Fig. 5f).

Tight junction structural abnormalities in mouse brains post-LIB exposure

Tight junctions connecting adjacent endothelial cells play key roles in maintaining the structural and functional integrity of the BBB [55]. Ultrastructural alternations of tight junctions, including discontinuities and openings were identified in cerebral ischemia [56]. In this study, most of the tight junctions appeared intact as a series of electron-dense zones sealing intercellular clefts in sham control mice (Fig. $6a_{1-2}$). By contrast, ultrastructural abnormalities of tight junctions were observed in LIB-exposed mice, including discontinuities, membrane-bound spaces, and vacuole formations at 7 and 30 DPI (Fig. $6a_{3-8}$). Quantitative analyses revealed percentages of intact tight junctions were lower in LIB-exposed mice compared to sham controls at 7 DPI (52.72% vs. 80.00%) and 30 DPI (51.51% vs. 78.05%) (Fig. 6b).

Levels of neurofilament light chain (Nf-L) and glial fibrillary acidic protein (GFAP) in mouse brain tissues and plasma post-LIB exposure

Brain tissue and circulating levels of neuronal and glial protein alterations in LIB-exposed mice were further estimated using the assays of FDA-approved biomarkers in TBI patients—Nf-L and GFAP. It was previously hypothesized that elevated serum levels of neuron- or glial-specific proteins, including neurofilaments indicate increased permeability of the BBB in blast-induced
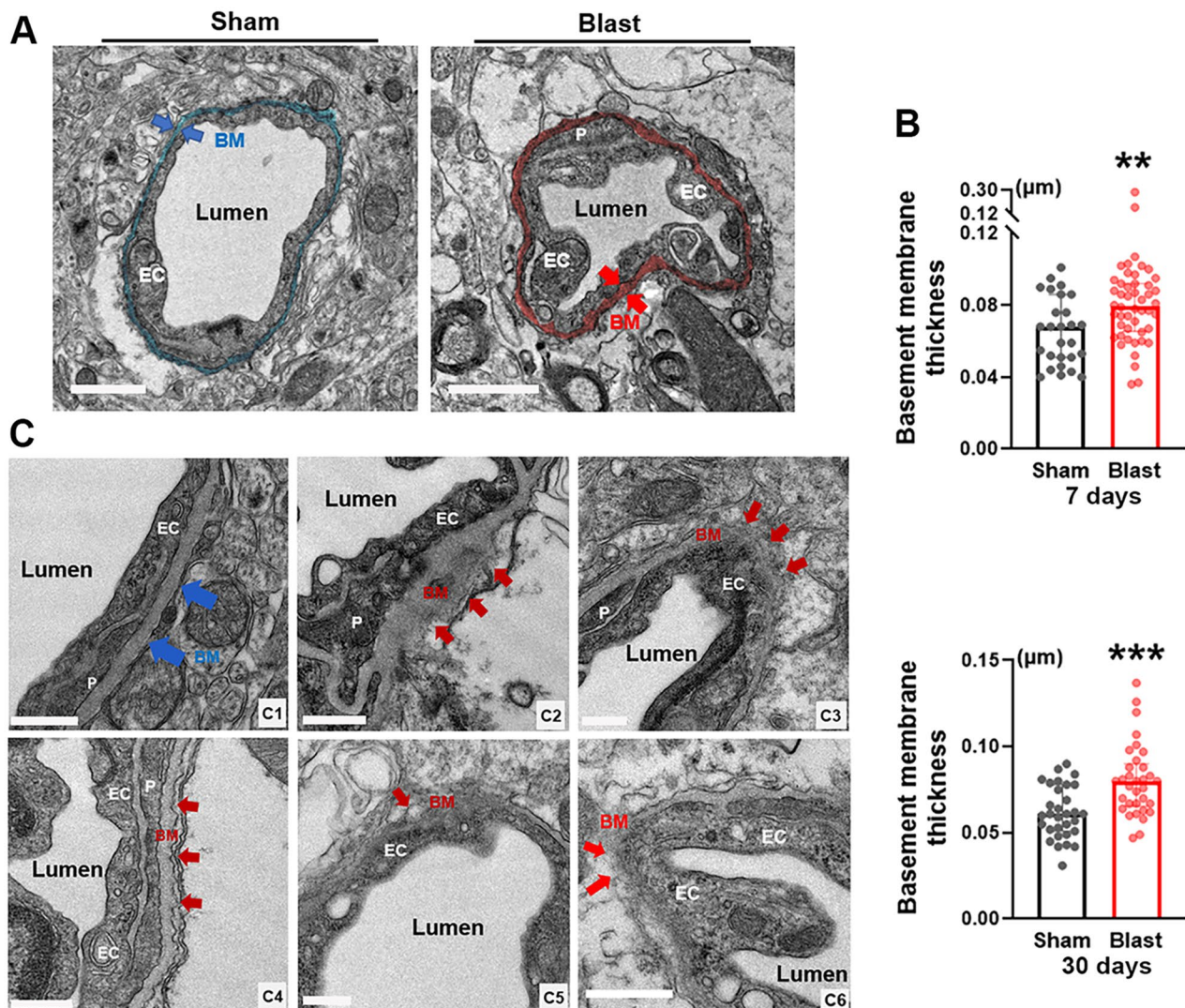
Fig. 4 Ultrastructural abnormalities of basement membranes in mouse brains post-LIB exposure. (**a**) Representative electron micrographs of microvessels in sham controls and LIB-exposed mice. Basement membranes (BM) are highlighted in blue in sham controls and pink in LIB-exposed mice at 7 DPI. Scale bar, 1 μm. (**b**) Quantifications of electron micrographs reveal basement membrane thickness in sham controls and LIB-exposed mice at 7 and 30 DPI. **, $p < 0.01$ and ***, $p < 0.001$. Data are expressed as median and interquartile range. (**c**) Blue arrows indicate normal basement membrane (BM) structure in sham control mice (c_1); red arrows indicate abnormal basement membrane structures in LIB-exposed mice with bulges (c_2), fragmentations (c_3), corrugations (c_4), and vacuoles within basement membranes (c_5) at 7 DPI, as well as fragmentations (c_6) at 30 DPI. Scale bar, 0.5 μm

TBI, in addition to neuronal and glial cell damage or loss [57]. It was also reported that higher levels of serum neurofilament levels were associated with greater impairment of BBB integrities in multiple sclerosis[58]. Tissue Nf-L was significantly elevated by 36.3% (mean values) in LIB-exposed mice compared to sham controls at 1 DPI, but not at 7 DPI and 3 months post injury; while plasma Nf-L was significantly elevated by 658.8% (mean values) in LIB-exposed mice compared to sham controls at 3 months post injury, but not at 1 and 7 DPI (Supplemental Fig. 2). In contrast no significant differences of tissue or plasma GFAP were identified in LIB-exposed mice

compared to sham controls at 1, 7 DPI and 3 months post injury (Supplemental Fig. 3).

Discussion

Previous NVU studies of bTBI mainly focused on moderate-to high-intensity blast exposure, repetitive blast exposure, or in conjunction with polytrauma [17, 20, 21, 59–64]. Since the majority of brain injuries in military personnel are classified as mild TBI [65], evaluations of NVU consequences in response to a single LIB provide an understanding of the pathophysiological impacts of mild TBI to help design therapeutic targets to minimize these injuries. In our recently established open-field,
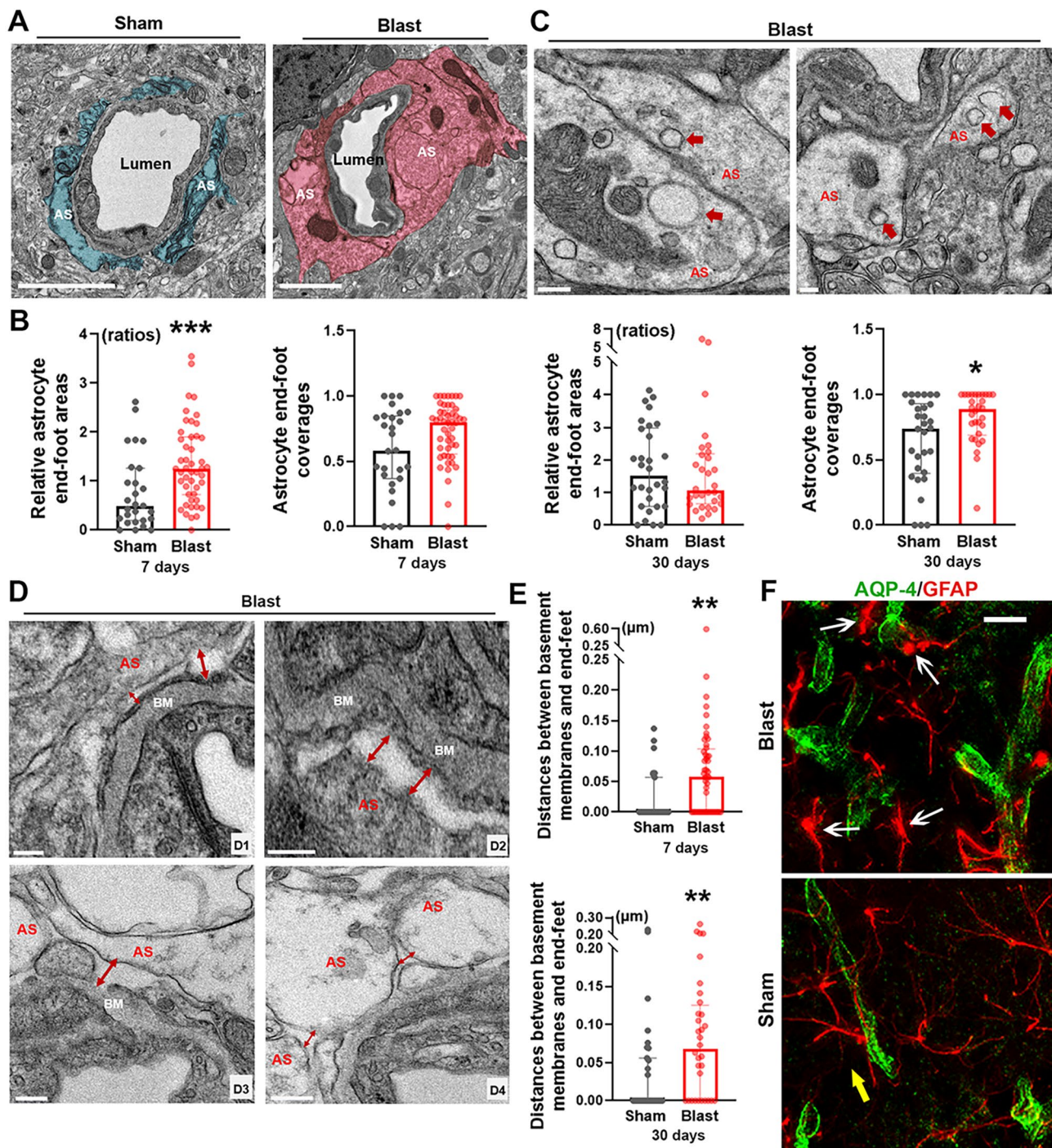
Fig. 5 Ultrastructural abnormalities of astrocyte end-feet and perivascular astrocyte reactivity in mouse brains post-LIB exposure. (**a**) Representative electron micrographs of microvessels in sham controls and LIB-exposed mice at 7 DPI. Astrocyte end-feet (AS) are highlighted in blue in sham controls and pink in LIB-exposed mice. Scale bar, 2 μm. (**b**) Quantifications of electron micrographs reveal astrocyte end-foot coverages and relative astrocyte end-foot areas in sham controls and LIB-exposed mice at 7 and 30 DPI. *, p < 0.05 and ***, p < 0.001. Data are expressed as median and interquartile range. (**c**) Red arrows indicate vacuoles within astrocyte end-feet (AS) in LIB-exposed mice at 7 DPI. Scale bar, 0.2 μm. (**d**) Red arrows indicate enlarged spaces between basement membranes (BM) and astrocyte end-feet (AS) (d_{1-3}) and between adjacent end-feet (d_4) in LIB-exposed mice at 7 DPI. Scale bar, 0.1 μm d_1, d_2 and 0.2 μm d_3, d_4. (**e**) Quantifications of electron micrographs reveal distances between basement membranes and astrocyte end-feet in sham controls and LIB-exposed mice at 7 and 30 DPI. **, p < 0.01. Data are expressed as median and interquartile range. (**f**) Photomicrographs of immunofluorescence staining with AQP-4 and GFAP showing perivascular astrocytes at 7 DPI. White arrows indicate reactive astrocytes in LIB-exposed mice, yellow arrows indicate non-reactive astrocytes in sham controls. Scale bar, 15 μm
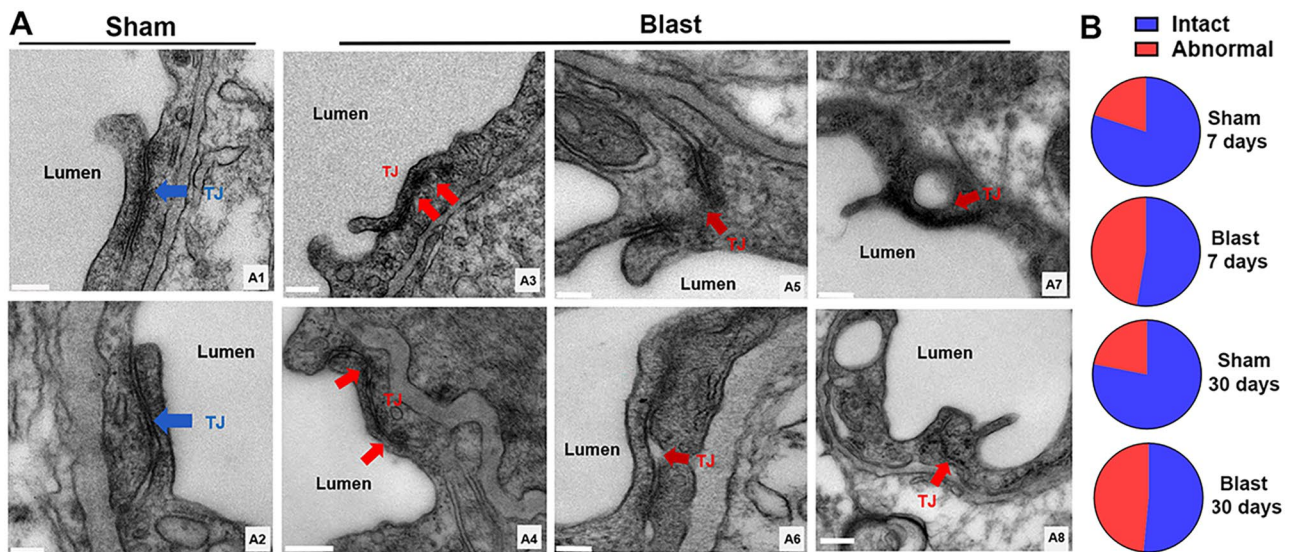
Fig. 6 Ultrastructural abnormalities of tight junctions in mouse brains post-LIB exposure. (**a**) Representative high resolution electron micrographs of microvessels in sham controls (a_1, a_2) and LIB-exposed mice at 7 (a_4, a_5, a_6, a_8) and 30 (a_3, a_7) DPI. Tight junctions (TJ) are indicated with blue arrows in sham controls and pink arrows in LIB-exposed mice. Scale bar, 0.2 μm a_1, a_3, a_4, a_5, a_7, a_8 and 0.5 μm a_2 and a_6. (**b**) Histograms show the percentages of intact and abnormal tight junctions in sham controls and LIB-exposed mice at 7 and 30 DPI.

non-inertial LIB mouse model with peak overpressure of 46.6 kPa, no brain damage was readily visible under light / fluorescence microscopes. However, nanoscale ultrastructural abnormalities, including defects in axonal myelin sheaths, mitochondria, and synapses were detected in LIB-exposed mice [23–25]. The present study clearly demonstrates damage in multiple cellular components of the NVU at the ultrastructural level, including luminal circularities of microvessels, pericytes, endothelial cells, basement membranes, astrocyte end-feet, and tight junctions post-LIB exposure, as well as vasomotor patterns with quantitative proteomics.

The UCLA Brain Injury Research Center Program reported that 45.2% of TBI patients had vasospasm from 2 to 13 DPI [66]. The incidence of vasospasm is also very high in patients with bTBI. Operation Iraqi Freedom (OIF) reported 47.4% of TBI patients (majority bTBI) suffered from vasospasm up to 30 DPI and with an average spasm duration of 14.3 DPI. Continued vasospasm was associated with higher mortality [67]. Using an in vitro blast model, Patrick W. Alford et al. demonstrated vascular hypercontractility and vascular smooth muscle phenotype switching [68]. Vasospasm was also identified in animal models of high-intensity blast exposure [21, 69, 70]. Here we extended studies to include details of luminal circularities of microvessels at the ultrastructural level. Quantitative analyses of electron micrographs revealed decreased lumen areas and increased lumen ratios in LIB-exposed mice at 7 DPI, indicating microvessel constrictions that correlate with these preclinical / clinical observations (Fig. 1).

The contraction of pericytes as the key regulator of microvessel diameters is Ca^{2+} dependent; thus, a rise of Ca^{2+} may evoke the constrictions of microvessels [71, 72]. Our proteomic investigation revealed significant upregulation of calcium-transporting ATPase (two isoforms) in LIB-exposed mice at 24 h post injury (Supplemental Fig. 1). It is reasonable to hypothesize that the disruption of Ca^{2+} hemostasis may be one of the mechanisms responsible for acute microvessel constrictions post-LIB exposure. Pericyte degeneration and disrupted pericyte-endothelial cell integrity also occur in TBI [73, 74]. Disruption of Ca^{2+} hemostasis may promote pericyte degeneration in LIB-exposed mice (Fig. 2). Compromised contractility of pericytes may thus contribute to microvessel dilation in LIB-exposed mice at 30 DPI (Fig. 1). Time-dependent cerebral vascular hyperreactivity in response to vasoactive mediators is another possible mechanism underlying vasomotor dysregulation [70]. Our proteomic study revealed significant downregulation of tyrosine 3-monooxygenase, serine / threonine-protein phosphatase (fragment) and serine / threonine-protein phosphatase PP1-alpha catalytic subunit, especially the predominant reduction of nitric oxide synthase (NOS) by 43.3% in LIB-exposed mice (Supplemental Fig. 1). These changes are consistent with previous reports, suggesting the NOS pathways play important roles in modifying cerebral blood flow after TBI [17, 75–78]. Further studies targeting Ca^{2+} and / or the NOS pathways may offer promising therapeutic strategies to mitigate the microvascular effects of LIB-induced mTBI.

Diffuse cerebral edema is one of the characteristic features of bTBI [79–82]. Herein, we identified swellings of

multiple NVU components induced by single LIB exposure (Figs. 3, 4 and 5). AQP-4, one of the most abundant water channels in the brain, is highly polarized to perivascular astrocytic end-feet. Altered expression and / or polarization of AQP-4 have been linked, both in experimental models and in humans, to impaired water homeostasis in neurological diseases such as ischemic stroke and neurotrauma [83–85], including bTBI [22, 64, 86]. In a previous study, peaks of AQP-4 expression were identified at 12 and 72 h and then decreased at 15 days post TBI [87], which may explain the swellings of endothelial cells and astrocyte end-feet were relatively more severe at 7 days post-injury than that at 30 days post-injury in LIB-exposed mice. Reactive astrocytes have been shown to induce loss of AQP-4 polarization [88, 89]. Herein, perivascular astrocytes showed somal hypertrophy and increased expression of GFAP –characteristic features of reactive astrocytes in LIB-exposed mice (Fig. 5) [54]. Reactive astrogliosis-associated AQP-4 modulation can be considered a potential mechanism of LIB-induced edema of NVU components. A previous immuno-gold study demonstrated that pericytes regulate AQP-4 anchoring to perivascular astrocyte end-feet [90]. Reduction of a pericyte marker, platelet-derived growth factor receptor β, has been linked to a loss of AQP-4 polarization and suppressed glymphatic system [91]. Our finding of pericyte degeneration in LIB-exposed mice (Fig. 2) suggests a potential role of dysregulated pericyte-mediated AQP-4 polarization as another possible mechanism underlying LIB-induced edema of NVU components.

The structural integrity and interactions between different NVU components are essential to the regulations of microvascular permeability and the dynamics of cerebral microcirculation [11, 92]. Tight junctions play essential roles in maintaining the integrity of the NVU by connecting adjacent endothelial cells. Reduced expressions of tight junction-specific proteins, including ZO-1, claudin-5, and occludin, have been reported in bTBI [64, 93–96]. In our current study, high magnification images captured by TEM helped us to confirm that single LIB exposure was able to induce ultrastructural abnormalities of tight junctions, such as tight junction discontinuities, membrane-bound spaces, and within vacuole formations (Fig. 6). Moreover, we found significantly enlarged distances between astrocyte end-feet and basement membranes (Fig. 5), indicating possible detachment of the NVU in the LIB-exposed mice.

The impaired integrity of NVU resulting in BBB damage in LIB-exposed mice was further supported by elevated circulating levels of Nf-L at 3 months post LIB exposure (Supplemental Fig. 2). It was demonstrated that BBB integrity was inversely proportional to the concentration of Nf-L in the plasma of humans [58]. Circulating levels of Nf-L are well-documented in clinical studies

as potential biomarkers of BBB damage and may predict clinical outcomes in TBI patients, including in the military population [97, 98]. Further studies estimating serum Nf-L alterations with therapeutic interventions in LIB models may aid in bench-to-bedside translational research of bTBI. In addition, we identified significantly elevated levels of Nf-L in acute phase (24 h) post LIB exposure (Supplemental Fig. 2). We speculated that NF-L might have been subjected to partial proteolysis[99, 100] and released into the more extractable pool. Though there were no significant changes in levels of the astrocytic biomarker GFAP in both cortical tissues and plasmas compared to sham controls (Supplemental Fig. 3) and by quantifying the fluorescent intensities of GFAP in the brain Sect. [24], as expected for the primary LIB conditions resulting in such "*invisible injury*", we indeed observed structural abnormalities of tight junctions and astrocyte end-foot detachment from basement membranes noted in the LIB-exposed mice (Fig. 5), supporting the notion of impaired NVU integrity post LIB exposure.

The extracellular matrix (ECM) is the biological scaffold material that maintains the integrity of the NVU by providing support and interactions between different NVU components [92, 101]. Activated matrix metalloproteinases (MMPs), especially gelatinases (MMP-2 / 9) were reported to mediate the degradation of ECM and tight junctions, leading to impaired integrity of the NVU [11, 102–105]. Our previous publications have demonstrated that SB-3CT, a specific gelatinase inhibitor, was able to restore NVU integrity, and subsequently, neurological functions in mice with severe TBI and ischemic stroke [11, 53, 102, 103]. Considering that upregulation and activation of gelatinases have been reported in bTBI by multiple research groups [22, 64, 106, 107], specific inhibition of gelatinases offers a potential therapeutic strategy in managing LIB-induced NVU damage.

Conclusion
Overall, our current study provides comprehensive quantitative and qualitative assessments of LIB-induced multi-component NVU abnormalities, potentially leading to widespread BBB impairments. The open-field blast model offers a potential platform for testing vascular interventions to minimize or mitigate primary LIB injury.

Abbreviations

mTBI	mild traumatic brain injury
LIB	low-intensity blast
TEM	transmission electron microscopy
NVU	neurovascular unit
Nf-L	neurofilament light chain
GFAP	glial fibrillary acidic protein
DPI	days post-injury
bTBI	blast-induced traumatic brain injury
CDC	Centers for Disease Control and Prevention
TBICoE	Traumatic Brain Injury Center of Excellence
DoD	US Defense Department

BBB	blood–brain barrier
MMP	matrix metalloproteinases
ARRIVE	animal research:reporting of in vivo experiments
i.p. injection	intraperitoneal injection
AQP-4	aquaporin-4
GFAP	glial fibrillary acidic protein
SDS	sodium dodecyl sulfate
TEAB	tetraethylammonium bicarbonate
PASEF	parallel accumulation–serial fragmentation
MS	mass spectrometry
NOS	nitric oxide synthase
OIF	Operation Iraqi Freedom
ECM	extracellular matrix

Supplementary Information

The online version contains supplementary material available at https://doi.org/10.1186/s40478-023-01636-4.

> **Supplemental Fig. 1.** Proteomic vasomotor alterations in mouse brains post-LIB exposure. Quantitative proteomics values (spectral counts) of vasomotor-related proteins with significant differences after LIB exposure. *, $p < 0.05$ and **, $p < 0.01$. Data are expressed as mean ± SD.
>
> **Supplemental Fig. 2.** Tissue and plasma levels of neurofilament light (Nf-L) in mouse brains post-LIB exposure. Quantification of Nf-L in brain tissue and plasma of sham controls and LIB-exposed mice at 1, 7 days and 3 months post injury. Nf-L levels in tissues (pg/µg) and in plasma (ng/ml) at 1 and 7 DPI and 3 months post-LIB are expressed mean ± SD; other data are expressed as median and interquartile range. *, $p < 0.05$ and **, $p < 0.01$. 24-hour tissue sham: n = 4, LIB: n = 6; 24-hour plasma sham: n = 5, LIB: n = 5; 7-day tissue sham: n = 10, LIB: n = 4; 7-day plasma sham: n = 3, LIB: n = 4; 3-month tissue sham: n = 6, LIB: n = 6; 3-month plasma sham: n = 5, LIB: n = 6.
>
> **Supplemental Fig. 3.** Tissue and plasma levels of glial fibrillary acidic protein (GFAP) in mouse brains post-LIB exposure. Quantification of GFAP in brain tissue and plasma of sham controls and LIB-exposed mice at 1, 7 days and 3 months post injury. Data are expressed as mean ± SD. 24-hour tissue sham: n = 4, LIB: n = 6; 24-hour plasma sham n = 5, LIB: n = 6; 7-day tissue sham: n = 10, LIB: n = 4; 7-day plasma sham: n = 3, LIB: n = 2; 3-month tissue sham: n = 6, LIB: n = 6; 3-month plasma sham: n = 6, LIB: n = 6.

Authors' contributions

Z.G. and J.C. designed research; C.L., S.C., H.S., D.G., P.L., A.B., F.K., J.C. and Z.G. performed research; C.L., S.C., P.L., A.B., M.J., A.Z., F.K., J.C. and Z.G. analyzed data; C.L., S.C., and Z.G. wrote the paper; P.L., C.M.G., M.J., F.K., K.W.W., R.G.D., I.C., and J.C. edited the paper; R.G.D. and I.C. provided insights on operational relevance and clinical translation; all authors read and approved the paper.

Data availability

The datasets used and/or analyzed during the current study are available from the corresponding author on request.

Declarations

Ethics approval and consent to participate

All animal experiments were performed in accordance with the University of Missouri-approved protocols for the Care and Use of Laboratory Animals and the Animal Research: Reporting of In Vivo Experiments (ARRIVE) guidelines.

Competing interests

The authors declared no potential conflicts of interest with respect to the research, authorship, and/or publication of this article.

References

1. Ralph G, David G, Howard R, Michael J (2005) Blast injuries. N Engl J Med 352(13):1335–1350
2. Siedhoff HR, Chen S, Song H, Cui J, Cernak I, Cifu DX, DePalma RG, Gu Z (2022) Perspectives on primary blast injury of the brain: translational insights into non-inertial low-intensity blast injury. Front Neurol 12:818169
3. Centers for Disease Control and Prevention, Comprehensive Listing (2022) ICD-10-CM Files, 2023 release of ICD-10-CM [https://www.cdc.gov/nchs/icd/Comprehensive-Listing-of-ICD-10-CM-Files.htm accessed 17 June 2022)]
4. Carr W, Stone JR, Walilko T, Young LA, Snook TL, Paggi ME, Tsao JW, Jankosky CJ, Parish RV, Ahlers ST (2016) Repeated low-level blast exposure: a descriptive human subjects study. Mil Med 181(5 Suppl):28–39
5. The Military Health System, Traumatic Brain Injury Center of Excellence (TBICoE) (2022) DoD Numbers for Tramatic Brain Injury Worldwide – Totals, 2000–2021 Q4 [https://health.mil/Military-Health-Topics/Conditions-and-Treatments/Traumatic-Brain-Injury/Worldwide-TBI-numbers accessed 17 June 2022).]
6. Barnes DE, Byers AL, Gardner RC, Seal KH, Boscardin WJ, Yaffe K (2018) Association of mild traumatic brain Injury with and without loss of consciousness with dementia in US Military Veterans. JAMA Neurol 75(9):1055–1061
7. Dirnagl U (2012) Pathobiology of injury after stroke: the neurovascular unit and beyond. Ann N Y Acad Sci 1268(1):21–25
8. Bell AH, Miller SL, Castillo-Melendez M, Malhotra A (2020) : The neurovascular unit: effects of brain insults during the perinatal period. Front NeuroSci :1452
9. Lo EH, Rosenberg GA (2009) The neurovascular unit in health and disease: introduction. Stroke 40(3 Suppl):S2–3
10. Sweeney MD, Ayyadurai S, Zlokovic BV (2016) Pericytes of the neurovascular unit: key functions and signaling pathways. Nat Neurosci 19(6):771–783
11. Chen S, Chen Z, Cui J, McCrary ML, Song H, Mobashery S, Chang M, Gu Z (2018) : Early Abrogation of Gelatinase Activity Extends the Time Window for tPA Thrombolysis after Embolic Focal Cerebral Ischemia in Mice. *eNeuro* 5(3)
12. Cui JK, Chen SY, Zhang CY, Meng FJ, Wu W, Hu R, Hadass O, Lehmidi T, Blair GJ, Lee M et al (2012) : Inhibition of MMP-9 by a selective gelatinase inhibitor protects neurovasculature from embolic focal cerebral ischemia. Mol Neurodegeneration 7
13. Chen S, Cui J, Jiang T, Olson ES, Cai QY, Yang M, Wu W, Guthrie JM, Robertson JD, Lipton SA et al (2017) Gelatinase activity imaged by activatable cell-penetrating peptides in cell-based and in vivo models of stroke. J Cereb Blood Flow Metab 37(1):188–200
14. Stanimirovic DB, Friedman A (2012) Pathophysiology of the neurovascular unit: disease cause or consequence? J Cereb Blood Flow Metab 32(7):1207–1221
15. Kawoos U, Gu M, Lankasky J, McCarron RM, Chavko M (2016) Effects of exposure to Blast overpressure on intracranial pressure and blood-brain barrier permeability in a rat model. PLoS ONE 11(12):e0167510
16. Rubovitch V, Ten-Bosch M, Zohar O, Harrison CR, Tempel-Brami C, Stein E, Hoffer BJ, Balaban CD, Schreiber S, Chiu WT et al (2011) A mouse model of blast-induced mild traumatic brain injury. Exp Neurol 232(2):280–289
17. Logsdon AF, Meabon JS, Cline MM, Bullock KM, Raskind MA, Peskind ER, Banks WA, Cook DG (2018) Blast exposure elicits blood-brain barrier disruption

and repair mediated by tight junction integrity and nitric oxide dependent processes. Sci Rep 8(1):11344

18. Kamnaksh A, Ahmed F, Kovesdi E, Barry ES, Grunberg NE, Long JB, Agoston DV (2014) Molecular mechanisms of increased cerebral vulnerability after repeated mild blast-induced traumatic brain injury. Transl Proteom 3:22–37

19. Kamnaksh A, Budde MD, Kovesdi E, Long JB, Frank JA, Agoston DV (2014) Diffusion tensor imaging reveals acute subcortical changes after mild blast-induced traumatic brain injury. Sci Rep 4:4809

20. Gama Sosa MA, De Gasperi R, Perez Garcia GS, Perez GM, Searcy C, Vargas D, Spencer A, Janssen PL, Tschiffely AE, McCarron RM et al (2019) Low-level blast exposure disrupts gliovascular and neurovascular connections and induces a chronic vascular pathology in rat brain. Acta Neuropathol Commun 7(1):6

21. Gama Sosa MA, De Gasperi R, Janssen PL, Yuk FJ, Anazodo PC, Pricop PE, Paulino AJ, Wicinski B, Shaughness MC, Maudlin-Jeronimo E et al (2014) Selective vulnerability of the cerebral vasculature to blast injury in a rat model of mild traumatic brain injury. Acta Neuropathol Commun 2:67

22. Abdul-Muneer PM, Schuetz H, Wang F, Skotak M, Jones J, Gorantla S, Zimmerman MC, Chandra N, Haorah J (2013) Induction of oxidative and nitrosative damage leads to cerebrovascular inflammation in an animal model of mild traumatic brain injury induced by primary blast. Free Radic Biol Med 60:282–291

23. Song H, Konan LM, Cui J, Johnson CE, Hubler GK, DePalma RG, Gu Z (2018) Nanometer ultrastructural brain damage following low intensity primary blast wave exposure. Neural Regen Res 13(9):1516–1519

24. Song H, Konan LM, Cui J, Johnson CE, Langenderfer M, Grant D, Ndam T, Simonyi A, White T, Demirci U et al (2018) Ultrastructural brain abnormalities and associated behavioral changes in mice after low-intensity blast exposure. Behav Brain Res 347:148–157

25. Konan LM, Song H, Pentecost G, Fogwe D, Ndam T, Cui J, Johnson CE, Grant D, White T, Chen M et al (2019) Multi-focal neuronal ultrastructural abnormalities and synaptic alterations in mice after low-intensity blast exposure. J Neurotrauma 36(13):2117–2128

26. Wang KK, Munoz Pareja JC, Mondello S, Diaz-Arrastia R, Wellington C, Kenney K, Puccio AM, Hutchison J, McKinnon N, Okonkwo DO et al (2021) Blood-based traumatic brain injury biomarkers - clinical utilities and regulatory pathways in the United States, Europe and Canada. Expert Rev Mol Diagn 21(12):1303–1321

27. Czeiter E, Amrein K, Gravesteijn BY, Lecky F, Menon DK, Mondello S, Newcombe VFJ, Richter S, Steyerberg EW, Vyvere TV et al (2020) Blood biomarkers on admission in acute traumatic brain injury: relations to severity, CT findings and care path in the CENTER-TBI study. EBioMedicine 56:102785

28. Song H, Cui J, Simonyi A, Johnson CE, Hubler GK, DePalma RG, Gu Z (2018) Linking blast physics to biological outcomes in mild traumatic brain injury: narrative review and preliminary report of an open-field blast model. Behav Brain Res 340:147–158

29. Song H, Chen M, Chen C, Cui J, Johnson CE, Cheng J, Wang X, Swerdlow RH, DePalma RG, Xia W et al (2019) Proteomic analysis and biochemical correlates of mitochondrial dysfunction after low-intensity primary blast exposure. J Neurotrauma 36(10):1591–1605

30. Chen M, Song H, Cui J, Johnson CE, Hubler GK, DePalma RG, Gu Z, Xia W (2018) Proteomic profiling of mouse brains exposed to Blast-Induced mild traumatic brain Injury reveals changes in Axonal Proteins and phosphorylated tau. J Alzheimers Dis 66(2):751–773

31. Siedhoff HR, Chen S, Balderrama A, Sun GY, Koopmans B, DePalma RG, Cui J, Gu Z (2022) Long-Term Effects of Low-Intensity Blast Non-Inertial Brain Injury on anxiety-like Behaviors in mice: home-cage monitoring assessments. Neurotrauma Rep 3(1):27–38

32. Chen S, Siedhoff HR, Zhang H, Liu P, Balderrama A, Li R, Johnson C, Greenlief CM, Koopmans B, Hoffman T Low-intensity blast induces acute glutamatergic hyperexcitability in mouse hippocampus leading to long-term learning deficits and altered expression of proteins involved in synaptic plasticity and serine protease inhibitors. Neurobiol Dis 2022:105634

33. Nahirney PC, Reeson P, Brown CE (2015) Ultrastructural analysis of blood–brain barrier breakdown in the peri-infarct zone in young adult and aged mice. J Cereb Blood Flow Metabolism 36(2):413–425

34. Xu J, Long H, Chen W, Cheng X, Yu H, Huang Y, Wang X, Li F (2018) Ultrastructural features of neurovascular units in a rat model of chronic compressive spinal cord injury. Front Neuroanat 11:136

35. Ceafalan LC, Fertig TE, Gheorghe TC, Hinescu ME, Popescu BO, Pahnke J, Gherghiceanu M (2019) Age-related ultrastructural changes of the basement membrane in the mouse blood-brain barrier. J Cell Mol Med 23(2):819–827

36. Black KL, Yin D, Ong JM, Hu J, Konda BM, Wang X, Ko MK, Bayan J-A, Sacapano MR, Espinoza A (2008) PDE5 inhibitors enhance tumor permeability and efficacy of chemotherapy in a rat brain tumor model. Brain Res 1230:290–302

37. Sántha P, Veszelka S, Hoyk Z, Mészáros M, Walter FR, Tóth AE, Kiss L, Kincses A, Oláh Z, Seprényi G (2016) Restraint stress-induced morphological changes at the blood-brain barrier in adult rats. Front Mol Neurosci 8:88

38. Cui Y, Liu P, Mooney BP, Franz AWE (2020) Quantitative proteomic analysis of Chikungunya Virus-Infected Aedes aegypti reveals proteome modulations indicative of persistent infection. J Proteome Res 19(6):2443–2456

39. Salehi A, Zhang JH, Obenaus A (2017) Response of the cerebral vasculature following traumatic brain injury. J Cereb Blood Flow Metab 37(7):2320–2339

40. Kramer DR, Winer JL, Pease BA, Amar AP, Mack WJ (2013) Cerebral vasospasm in traumatic brain injury. Neurol Res Int 2013:415813

41. Wang KK, Yang Z, Zhu T, Shi Y, Rubenstein R, Tyndall JA, Manley GT (2018) An update on diagnostic and prognostic biomarkers for traumatic brain injury. Expert Rev Mol Diagn 18(2):165–180

42. Badhwar A, Stanimirovic DB, Hamel E, Haqqani AS (2014) The proteome of mouse cerebral arteries. J Cereb Blood Flow Metab 34(6):1033–1046

43. Hamilton NB, Attwell D, Hall CN (2010) : Pericyte-mediated regulation of capillary diameter: a component of neurovascular coupling in health and disease. Front Neuroenergetics 2

44. Gonzales AL, Klug NR, Moshkforoush A, Lee JC, Lee FK, Shui B, Tsoukias NM, Kotlikoff MI, Hill-Eubanks D, Nelson MT (2020) Contractile pericytes determine the direction of blood flow at capillary junctions. Proc Natl Acad Sci 117(43):27022–27033

45. Uemura MT, Maki T, Ihara M, Lee VMY, Trojanowski JQ (2020) Brain microvascular Pericytes in Vascular Cognitive Impairment and Dementia. Front Aging Neurosci 12:80

46. Ding R, Hase Y, Ameen-Ali KE, Ndung'u M, Stevenson W, Barsby J, Gourlay R, Akinyemi T, Akinyemi R, Uemura MT et al (2020) Loss of capillary pericytes and the blood-brain barrier in white matter in poststroke and vascular dementias and Alzheimer's disease. Brain Pathol 30(6):1087–1101

47. Krueger M, Mages B, Hobusch C, Michalski D (2019) Endothelial edema precedes blood-brain barrier breakdown in early time points after experimental focal cerebral ischemia. Acta Neuropathol Commun 7(1):1–17

48. Kang M, Yao Y (2020) Basement membrane changes in ischemic stroke. Stroke 51(4):1344–1352

49. Ito U, Hakamata Y, Kawakami E, Oyanagi K (2011) Temporary [corrected] cerebral ischemia results in swollen astrocytic end-feet that compress microvessels and lead to delayed [corrected] focal cortical infarction. J Cereb Blood Flow Metab 31(1):328–338

50. Hayden MR (2019) Hypothesis: astrocyte foot processes detachment from the neurovascular unit in Female Diabetic mice may impair modulation of Information Processing—Six degrees of separation. Brain Sci 9(4):83

51. Yamashita T, Kamiya T, Deguchi K, Inaba T, Zhang H, Shang J, Miyazaki K, Ohtsuka A, Katayama Y, Abe K (2009) Dissociation and protection of the neurovascular unit after thrombolysis and reperfusion in ischemic rat brain. J Cereb Blood Flow Metabolism 29(4):715–725

52. Jayaraj RL, Azimullah S, Beiram R, Jalal FY, Rosenberg GA (2019) Neuroinflammation: friend and foe for ischemic stroke. J Neuroinflamm 16(1):1–24

53. Hadass O, Tomlinson BN, Gooyit M, Chen S, Purdy JJ, Walker JM, Zhang C, Giritharan AB, Purnell W, Robinson CR (2013) Selective inhibition of matrix metalloproteinase-9 attenuates secondary damage resulting from severe traumatic brain injury. PLoS ONE 8(10):e76904

54. Canchi S, Sarntinoranont M, Hong Y, Flint JJ, Subhash G, King MA (2017) Simulated blast overpressure induces specific astrocyte injury in an ex vivo brain slice model. PLoS ONE 12(4):e0175396

55. Luissint A-C, Artus C, Glacial F, Ganeshamoorthy K, Couraud P-O (2012) Tight junctions at the blood brain barrier: physiological architecture and disease-associated dysregulation. Fluids and Barriers of the CNS 9(1):1–12

56. Li J, Li C, Yuan W, Wu J, Li J, Li Z, Zhao Y (2017) Mild hypothermia alleviates brain oedema and blood-brain barrier disruption by attenuating tight junction and adherens junction breakdown in a swine model of cardiopulmonary resuscitation. PLoS ONE 12(3):e0174596

57. Agoston DV, Elsayed M (2012) Serum-based protein biomarkers in blast-induced traumatic brain injury spectrum disorder. Front Neurol 3:107

58. Uher T, McComb M, Galkin S, Srpova B, Oechtering J, Barro C, Tyblova M, Bergsland N, Krasensky J, Dwyer M et al (2021) Neurofilament levels are associated with blood-brain barrier integrity, lymphocyte extravasation, and risk factors following the first demyelinating event in multiple sclerosis. Mult Scler 27(2):220–231

Li *et al. Acta Neuropathologica Communications*   (2023) 11:144

Page 14 of 15

59. Yeoh S, Bell ED, Monson KL (2013) Distribution of blood-brain barrier disruption in primary blast injury. Ann Biomed Eng 41(10):2206–2214

60. Hue CD, Cho FS, Cao S, Nicholls RE, Vogel Iii EW, Sibindi C, Arancio O, Dale Bass CR, Meaney DF (2016) Morrison Iii B: time course and size of blood-brain barrier opening in a mouse model of Blast-Induced Traumatic Brain Injury. J Neurotrauma 33(13):1202–1211

61. Meabon JS, Huber BR, Cross DJ, Richards TL, Minoshima S, Pagulayan KF, Li G, Meeker KD, Kraemer BC, Petrie EC et al (2016) Repetitive blast exposure in mice and combat veterans causes persistent cerebellar dysfunction. Sci Transl Med 8(321):321ra326

62. Shetty AK, Mishra V, Kodali M, Hattiangady B (2014) Blood brain barrier dysfunction and delayed neurological deficits in mild traumatic brain injury induced by blast shock waves. Front Cell Neurosci 8:232

63. Elder GA, Gama Sosa MA, De Gasperi R, Stone JR, Dickstein DL, Haghighi F, Hof PR, Ahlers ST (2015) Vascular and inflammatory factors in the pathophysiology of blast-induced brain injury. Front Neurol 6:48

64. Kawoos U, Abutarboush R, Gu M, Chen Y, Statz JK, Goodrich SY, Ahlers ST (2021) Blast-induced temporal alterations in blood–brain barrier properties in a rodent model. Sci Rep 11(1):1–15

65. Chapman JC, Diaz-Arrastia R (2014) Military traumatic brain injury: a review. Alzheimer's Dement 10:S97–S104

66. Oertel M, Boscardin WJ, Obrist WD, Glenn TC, McArthur DL, Gravori T, Lee JH, Martin NA (2005) Posttraumatic vasospasm: the epidemiology, severity, and time course of an underestimated phenomenon: a prospective study performed in 299 patients. J Neurosurg 103(5):812–824

67. Armonda RA, Bell RS, Vo AH, Ling G, DeGraba TJ, Crandall B, Ecklund J, Campbell WW (2006) Wartime traumatic cerebral vasospasm: recent review of combat casualties. Neurosurgery 59(6):1215–1225 discussion 1225

68. Alford PW, Dabiri BE, Goss JA, Hemphill MA, Brigham MD, Parker KK (2011) Blast-induced phenotypic switching in cerebral vasospasm. Proc Natl Acad Sci U S A 108(31):12705–12710

69. Valiyaveettil M, Alamneh Y, Wang Y, Arun P, Oguntayo S, Wei Y, Long JB, Nambiar MP (2013) Contribution of systemic factors in the pathophysiology of repeated blast-induced neurotrauma. Neurosci Lett 539:1–6

70. Abutarboush R, Gu M, Kawoos U, Mullah SH, Chen Y, Goodrich SY, Lashof-Sullivan M, McCarron RM, Statz JK, Bell RS (2019) Exposure to blast overpressure impairs cerebral microvascular responses and alters vascular and astrocytic structure. J Neurotrauma 36(22):3138–3157

71. Dalkara T, Gursoy-Ozdemir Y, Yemisci M (2011) Brain microvascular pericytes in health and disease. Acta Neuropathol 122(1):1–9

72. Cheng J, Korte N, Nortley R, Sethi H, Tang Y, Attwell D (2018) Targeting pericytes for therapeutic approaches to neurological disorders. Acta Neuropathol 136(4):507–523

73. Ojo J, Eisenbaum M, Shackleton B, Lynch C, Joshi U, Saltiel N, Pearson A, Ringland C, Paris D, Mouzon B et al (2021) Mural cell dysfunction leads to altered cerebrovascular tau uptake following repetitive head trauma. Neurobiol Dis 150:105237

74. Bhowmick S, D'Mello V, Caruso D, Wallerstein A, Abdul-Muneer PM (2019) Impairment of pericyte-endothelium crosstalk leads to blood-brain barrier dysfunction following traumatic brain injury. Exp Neurol 317:260–270

75. Logsdon AF, Schindler AG, Meabon JS, Yagi M, Herbert MJ, Banks WA, Raskind MA, Marshall DA, Keene CD, Perl DP (2020) Nitric oxide synthase mediates cerebellar dysfunction in mice exposed to repetitive blast-induced mild traumatic brain injury. Sci Rep 10(1):1–14

76. Villalba N, Sonkusare SK, Longden TA, Tran TL, Sackheim AM, Nelson MT, Wellman GC, Freeman K (2014) Traumatic brain injury disrupts cerebrovascular tone through endothelial inducible nitric oxide synthase expression and nitric oxide gain of function. J Am Heart Association 3(6):e001474

77. Terpolilli NA, Kim SW, Thal SC, Kuebler WM, Plesnila N (2013) Inhaled nitric oxide reduces secondary brain damage after traumatic brain injury in mice. J Cereb Blood Flow Metab 33(2):311–318

78. Garry PS, Ezra M, Rowland MJ, Westbrook J, Pattinson KT (2015) The role of the nitric oxide pathway in brain injury and its treatment–from bench to bedside. Exp Neurol 263:235–243

79. Miller ST, Cooper CF, Elsbernd P, Kerwin J, Mejia-Alvarez R, Willis AM (2021) : Localizing clinical patterns of Blast traumatic brain Injury through Computational modeling and Simulation. Front Neurol 12

80. Ling G, Bandak F, Armonda R, Grant G, Ecklund J (2009) Explosive blast neurotrauma. J Neurotrauma 26(6):815–825

81. Hicks RR, Fertig SJ, Desrocher RE, Koroshetz WJ, Pancrazio JJ (2010) Neurological effects of blast injury. J trauma 68(5):1257

82. Goldstein LE, Fisher AM, Tagge CA, Zhang XL, Velisek L, Sullivan JA, Upreti C, Kracht JM, Ericsson M, Wojnarowicz MW et al (2012) Chronic traumatic encephalopathy in blast-exposed military veterans and a blast neurotrauma mouse model. Sci Transl Med 4(134):134ra160

83. Aoki K, Uchihara T, Tsuchiya K, Nakamura A, Ikeda K, Wakayama Y (2003) Enhanced expression of aquaporin 4 in human brain with infarction. Acta Neuropathol 106(2):121–124

84. Mader S, Brimberg L (2019) : Aquaporin-4 Water Channel in the brain and its implication for Health and Disease. Cells 8(2)

85. Iliff JJ, Chen MJ, Plog BA, Zeppenfeld DM, Soltero M, Yang L, Singh I, Deane R, Nedergaard M (2014) Impairment of glymphatic pathway function promotes tau pathology after traumatic brain injury. J Neurosci 34(49):16180–16193

86. Clark AT, Abrahamson EE, Harper MM, Ikonomovic MD (2022) Chronic effects of blast injury on the microvasculature in a transgenic mouse model of Alzheimer's disease related Aβ amyloidosis. Fluids and Barriers of the CNS 19(1):1–15

87. Xiong A, Xiong R, Yu J, Liu Y, Liu K, Jin G, Xu J, Yan J (2021) Aquaporin-4 is a potential drug target for traumatic brain injury via aggravating the severity of brain edema. Burns Trauma 9:tkaa050

88. Chen T, Lennon VA, Liu YU, Bosco DB, Li Y, Yi M-H, Zhu J, Wei S, Wu L-J (2020) Astrocyte-microglia interaction drives evolving neuromyelitis optica lesion. J Clin Investig 130(8):4025–4038

89. Dai J, Lin W, Zheng M, Liu Q, He B, Luo C, Lu X, Pei Z, Su H, Yao X (2017) Alterations in AQP4 expression and polarization in the course of motor neuron degeneration in SOD1G93A mice. Mol Med Rep 16(2):1739–1746

90. Gundersen GA, Vindedal GF, Skare Ø, Nagelhus EA (2014) Evidence that pericytes regulate aquaporin-4 polarization in mouse cortical astrocytes. Brain Struct Function 219(6):2181–2186

91. Munk AS, Wang W, Bechet NB, Eltanahy AM, Cheng AX, Sigurdsson B, Benraiss A, Mae MA, Kress BT, Kelley DH et al (2019) PDGF-B is required for development of the Glymphatic System. Cell Rep 26(11):2955–2969e2953

92. Chen S, Song H, Cui J, Shenker JI, Chen Y, Sun GY, Feng H, Gu Z (2018) Gelatinase-mediated impairment of Microvascular Beds in Cerebral Ischemia and Reperfusion Injury. Cerebral ischemic reperfusion injuries (CIRI). edn.: Springer, pp 1–14

93. Heyburn L, Abutarboush R, Goodrich S, Urioste R, Batuure A, Wheel J, Wilder DM, Arun P, Ahlers ST, Long JB (2021) Repeated low-level blast acutely alters brain cytokines, neurovascular proteins, mechanotransduction, and neurodegenerative markers in a rat model. Front Cell Neurosci 15:26

94. Hue CD, Cho FS, Cao S, Bass CRD, Meaney DF, Morrison B III (2015) Dexamethasone potentiates in vitro blood-brain barrier recovery after primary blast injury by glucocorticoid receptor-mediated upregulation of ZO-1 tight junction protein. J Cereb Blood Flow Metabolism 35(7):1191–1198

95. Hue CD, Cao S, "Dale" Bass CR, Meaney DF, Morrison B III (2014) Repeated primary blast injury causes delayed recovery, but not additive disruption, in an in vitro blood–brain barrier model. J Neurotrauma 31(10):951–960

96. Hue CD, Cao S, Haider SF, Vo KV, Effgen GB, Vogel E III, Panzer MB, Bass CRD, Meaney DF (2013) Morrison III B: blood-brain barrier dysfunction after primary blast injury in vitro. J Neurotrauma 30(19):1652–1663

97. Guedes VA, Lange RT, Lippa SM, Lai C, Greer K, Mithani S, Devoto C, K AE, Wagner CL, Martin CA et al (2022) Extracellular vesicle neurofilament light is elevated within the first 12-months following traumatic brain injury in a U.S military population. Sci Rep 12(1):4002

98. Shahim P, Politis A, van der Merwe A, Moore B, Ekanayake V, Lippa SM, Chou YY, Pham DL, Butman JA, Diaz-Arrastia R et al (2020) Time course and diagnostic utility of NfL, tau, GFAP, and UCH-L1 in subacute and chronic TBI. Neurology 95(6):e623–e636

99. Buki A, Koizumi H, Povlishock JT (1999) Moderate posttraumatic hypothermia decreases early calpain-mediated proteolysis and concomitant cytoskeletal compromise in traumatic axonal injury. Exp Neurol 159(1):319–328

100. Posmantur RM, Zhao X, Kampfl A, Clifton GL, Hayes RL (1998) Immunoblot analyses of the relative contributions of cysteine and aspartic proteases to neurofilament breakdown products following experimental brain injury in rats. Neurochem Res 23(10):1265–1276

101. Badylak SF, Freytes DO, Gilbert TW (2009) Extracellular matrix as a biological scaffold material: structure and function. Acta Biomater 5(1):1–13

102. Cui J, Chen S, Zhang C, Meng F, Wu W, Hu R, Hadass O, Lehmidi T, Blair GJ, Lee M et al (2012) Inhibition of MMP-9 by a selective gelatinase inhibitor protects neurovasculature from embolic focal cerebral ischemia. Mol Neurodegen 7:21

103. Gu Z, Cui J, Brown S, Fridman R, Mobashery S, Strongin AY, Lipton SA (2005) A highly specific inhibitor of matrix metalloproteinase-9 rescues laminin from

proteolysis and neurons from apoptosis in transient focal cerebral ischemia. J Neurosci 25(27):6401–6408

104. Rempe RG, Hartz AM, Bauer B (2016) Matrix metalloproteinases in the brain and blood–brain barrier: versatile breakers and makers. J Cereb Blood Flow Metabolism 36(9):1481–1507

105. Yang Y, Estrada EY, Thompson JF, Liu W, Rosenberg GA (2007) Matrix metalloproteinase-mediated disruption of tight junction proteins in cerebral vessels is reversed by synthetic matrix metalloproteinase inhibitor in focal ischemia in rat. J Cereb Blood Flow Metabolism 27(4):697–709

106. Ravin R, Blank PS, Busse B, Ravin N, Vira S, Bezrukov L, Waters H, Guerrero-Cazares H, Quinones-Hinojosa A, Lee PR (2016) Blast shockwaves propagate Ca2 + activity via purinergic astrocyte networks in human central nervous system cells. Sci Rep 6(1):1–14

107. Kuriakose M, Younger D, Ravula AR, Alay E, Rama Rao KV, Chandra N (2019) Synergistic role of oxidative stress and blood-brain barrier permeability as injury mechanisms in the acute pathophysiology of blast-induced neurotrauma. Sci Rep 9(1):1–12

Publisher's Note